Dynamics-aware Optimal Operation of Microgrids in Islanded Mode

Roohallah Khatami, Bo Chen, and Yu Christine Chen
Department of Electrical and Computer Engineering
The University of British Columbia
Vancouver, BC, Canada
Email: {roohallah.khatami, cbhp1993, chen}@ece.ubc.ca

***Abstract*—This paper formulates a dynamics-aware linearized optimal power flow (OPF) problem that co-optimizes operation cost and frequency regulation of islanded microgrids in response to load disturbances. The proposed dynamics-aware model penalizes frequency deviations in the objective function, thus tracking the system frequency to synchronous value in steady state by suitably updating generator reference set-points. The use of linearized power flow constraints promotes computational practicality while maintaining sufficient modelling fidelity. We demonstrate the benefits of the proposed model via numerical case studies involving an 18-Bus AC shipboard test system serving as a practical instance of an islanded microgrid.**

***Index Terms*—Frequency dynamics, frequency regulation, islanded microgrids, linearized model, optimal power flow**

I. Introduction

Equipped with local generation as well as autonomous control capability, a microgrid can operate in both grid-connected and islanded modes. This unique property renders microgrids indispensable actuators in the modern electric power systems, key components for improving energy efficiency and power reliability, and enablers of integrating aspirational shares of renewable generation [1]. The undeniable benefits on offer have spurred efforts by system operators and policy makers to facilitate microgrid integration in power systems [2], and the associated cumulative revenue is anticipated to reach above $\$164.8$ billion by 2024 [3]. Moreover, microgrids in the islanded mode are representative of hybrid-electric shipboard power systems, and marine transportation is absolutely essential in the global economy as more than 90% of trade goods are carried by sea [4]. There are, however, significant technical challenges to operating microgrids in a reliable and economical fashion. Notably, the smaller size of microgrids as compared to the bulk power system suggests more conservative operation and control strategies, especially in the islanded mode when microgrids are left with reduced inertia and become more susceptible to larger frequency excursions due to load fluctuations [5]. However, conservative strategies are typically at odds with operating the system in the most cost effective manner.

While there have been many proposed designs of microgrid control systems over the past decades, the hierarchical architecture remains the dominating strategy [6]. This architecture embeds three control layers—primary, secondary, and tertiary—that trigger sequentially across different timescales [7]. Primary control refers to local voltage and frequency control of generation sources that takes effect within seconds after a disturbance like a load change. In case of sustained generation-load imbalance, primary frequency control results in steady-state frequency deviations that are, in turn, regulated by secondary control through automatic generation control (AGC). The AGC updates generator references every few seconds based on the measured frequency deviation and the optimal set-points furnished by tertiary control. In the tertiary control layer, the optimal generator set-points are determined by solving an economic dispatch (ED) that minimizes the microgrid operation cost given the look-ahead predicted system load. The AGC adjusts the generator reference power inputs in real time based on small-signal sensitivity analysis around the optimal ED set-points, which indeed perform well for small load variations [8]. However, for more aggressive load changes, the underlying small-signal assumptions may no longer hold, and the AGC action may lead to economically inefficient operation. Thus, given that the net-load (load minus non-dispatchable generation) of low-inertia islanded microgrids hosting high shares of renewable resources undergoes larger and more frequent variations, embedding ED in lower control layers holds latent potential for cost reductions.

Co-optimization of energy dispatch and frequency regulation has recently been studied from several perspectives [9]–[15]. For example, [9] shows that the AGC function combined with system dynamics is indeed the equilibrium point of a suitably designed optimization problem, inspiring a reverse-engineering approach that breaks the control hierarchy and incorporates ED into secondary control. In contrast, the focus of [10] is to preserve the multi-time-scale control architecture by formulating a two-stage stochastic optimization problem temporally decomposed over secondary and tertiary control layers. Real-time dynamic pricing is utilized in [11], [12] to envision an iterative market for real-time energy dispatch, which results in an efficient market equilibrium with zero steady-state frequency deviation. In [13], the security-constrained ED is enhanced with the AGC model in an effort to co-optimize three distinct services: energy, spinning reserve, and regulation capacity. A dynamics-aware continuous-time ED problem is formulated in [14] along with a computationally efficient function space-based solution method, and it improves economic efficiency and system frequency by providing con-

tinuously differentiable optimal dispatch inputs for the AGC. The papers cited above either completely neglect network constraints [14] or use overly simplified network models, such as the DC power flow [10], [13] or a similar model except without the unity voltage assumption [9], [12]. Notably, [9]–[14] all disregard network losses. While the lossless assumption may be applicable for high-voltage transmission systems, it is unrealistic for typical microgrids operating at lower voltages. To overcome this limitation, [15] adopts a more elaborate network model derived from linearizing the power flow equations around a *known* operating point.

In this paper, we formulate a comprehensive dynamics-aware optimal power flow (OPF) problem for microgrid operation in the islanded mode. Salient features of the formulated problem include: (i) generator dynamics as constraints, (ii) two distinct time steps to concurrently model slower generator set-point decisions and faster system dynamics, and (iii) penalization of frequency excursions (from synchronous value) in the objective function to mimic AGC functionality. To capture network constraints, we leverage a linearized power flow model that accommodates non-unity voltage magnitudes, accounts for reactive-power flows and injections, and incorporates line losses as lumped loads distributed between line sending and receiving ends. Unlike [15], the linearization in our formulation does not require a known operating point. The linearized power flow constraints promote computational efficiency in the solution algorithm. The resulting linear programming (LP) problem can be solved using well established algorithms that are readily available in standard optimization toolboxes. Given the above, compared to prior work in this domain, our proposed problem formulation strikes a tactful balance between modelling fidelity and computational practicality.

II. Preliminaries

The proposed dynamics-aware formulation incorporates synchronous generator dynamics in an OPF problem. In this section, we present models for linearized AC power flow constraints and synchronous generator dynamics.

A. Linearized AC Power Flow Model

Consider a microgrid modelled as a directed graph $(\mathcal{N}, \mathcal{E})$, where $\mathcal{N} = \{1, \dots, N\}$ and $\mathcal{E} = \{(i,j), i,j \in \mathcal{N}, j \equiv j(i)\}$ respectively represent the sets of nodes and lines. For node $i \in \mathcal{N}$, denote its voltage magnitude and phase angle by V_i and θ_i, respectively. We model the line $(i,j) \in \mathcal{E}$ using the lumped-parameter Π-model with series admittance $y_{ij} = y_{ji} = g_{ij} + \mathrm{j}b_{ij}$ and shunt admittance $y_{ij}^{\mathrm{sh}} = y_{ji}^{\mathrm{sh}} = \mathrm{j}b_{ij}^{\mathrm{sh}}$. Let $\mathcal{G}$ denote the set of online generators. Generator $g \in \mathcal{G}$ delivers active power P_g^{e} and reactive power Q_g^{e}. Taken together, generators supply non-frequency-sensitive active- and reactive-power loads in the microgrid P_i^{d} and Q_i^{d}, $i \in \mathcal{N}$. Finally denote the set of online generators connected to node i by $\mathcal{G}_i$.

1) Line Power Flows: The nonlinear equations describing the active- and reactive-power flows in line $(i,j) \in \mathcal{E}$ are respectively given by

$$P_{ij} = V_i^2 g_{ij} - V_i V_j \left(g_{ij} \cos\theta_{ij} + b_{ij} \sin\theta_{ij}\right), \quad (1)$$

$$Q_{ij} = -V_i^2 (b_{ij} + b_{ij}^{\mathrm{sh}}) + V_i V_j \left(b_{ij} \cos\theta_{ij} - g_{ij} \sin\theta_{ij}\right), \quad (2)$$

where $\theta_{ij} := \theta_i - \theta_j$. Assume that $\theta_{ij} \ll 1$, so that $\sin\theta_{ij} \approx \theta_{ij}$ and $\cos\theta_{ij} \approx 1$ in (1) and (2). Also we substitute $V_i = 1 + \Delta V_i$, $i \in \mathcal{N}$, into (1)–(2) to approximate line active- and reactive-power flows as follows:

$$P_{ij} = (\Delta V_i - \Delta V_j)\, g_{ij} - b_{ij}\theta_{ij}, \quad (3)$$

$$Q_{ij} = -(1 + 2\Delta V_i) b_{ij}^{\mathrm{sh}} - (\Delta V_i - \Delta V_j)\, b_{ij} - g_{ij}\theta_{ij}, \quad (4)$$

where we have neglected the quadratic terms [16]. In general, variables in (3)–(4) may be subject to the following box constraints:

$$\underline{P}_{ij} \le P_{ij} \le \overline{P}_{ij},\ (i,j) \in \mathcal{E}, \quad (5)$$

$$\underline{Q}_{ij} \le Q_{ij} \le \overline{Q}_{ij},\ (i,j) \in \mathcal{E}, \quad (6)$$

$$\Delta\underline{V}_i \le \Delta V_i \le \Delta\overline{V}_i,\ i \in \mathcal{N}, \quad (7)$$

capturing, respectively, limits in line active-power flows, line reactive-power flows, and nodal voltage magnitudes.

2) Line Losses: Consistent with the power flow model in [16], to model losses in line $(i,j) \in \mathcal{E}$, we apply the second-order Taylor series expansion of $\cos\theta_{ij} \approx 1 - \theta_{ij}^2/2$ and further neglect all higher-order terms in the expression for line losses. Then the active-power losses in line (i,j) can be approximated by the following quadratic function:

$$P_{ij}^{\mathrm{loss}} = g_{ij}\theta_{ij}^2,\ (i,j) \in \mathcal{E}, \quad (8)$$

which we aim to linearize. Given that the quadratic loss function in (8) is convex in θ_{ij}, and the minimization of loss aligns with that of operation cost, an approach analogous to prevailing cost function linearization (see, e.g., [17]) may be applied, except with an extra set of auxiliary variables to capture the absolute value of θ_{ij}. To this end, let us define positive-valued auxiliary variables θ_{ij}^+ and θ_{ij}^- so that $\theta_{ij} = \theta_{ij}^+ - \theta_{ij}^-$. Also define a linearization domain such that its minimum and maximum bounds are marked by 0 to $\overline{\theta}_{ij}$ (where $\overline{\theta}_{ij}$ is a sufficiently large value that does not restrict the space of feasible solutions) and divide the interval 0 to $\overline{\theta}_{ij}$ into S linearization segments $\mathcal{S} = \{1, \dots, S\}$. Each segment $s \in \mathcal{S}$ is delimited by its boundary values $\widehat{\theta}_{ij,s-1}$ and $\widehat{\theta}_{ij,s}$ such that $[0, \overline{\theta}_{ij}] = \bigcup_{s\in\mathcal{S}} [\widehat{\theta}_{ij,s-1}, \widehat{\theta}_{ij,s}]$, where $\widehat{\theta}_{ij,0} = 0$ and $\widehat{\theta}_{ij,S} = \overline{\theta}_{ij}$. Further define the positive-valued auxiliary variable $\vartheta_{ij,s}$, $s \in \mathcal{S}$, so that $0 \le \vartheta_{ij,s} \le \widehat{\theta}_{ij,s} - \widehat{\theta}_{ij,s-1}$. Let $\alpha_{ij,s}$ represent the slope of linearized loss function in segment $s \in \mathcal{S}$, which can be expressed as

$$\alpha_{ij,s} = \frac{g_{ij}\widehat{\theta}_{ij,s}^2 - g_{ij}\widehat{\theta}_{ij,s-1}^2}{\widehat{\theta}_{ij,s} - \widehat{\theta}_{ij,s-1}} = g_{ij}(\widehat{\theta}_{ij,s} + \widehat{\theta}_{ij,s-1}). \quad (9)$$

Then the loss function in (8) can be linearized as follows:

$$P_{ij}^{\mathrm{loss}} = \sum_{s\in\mathcal{S}} \alpha_{ij,s}\vartheta_{ij,s},\ (i,j) \in \mathcal{E}, \quad (10)$$

$$\theta_{ij} = \theta_{ij}^+ - \theta_{ij}^-,\ \theta_{ij}^+, \theta_{ij}^- \ge 0,\ (i,j) \in \mathcal{E}, \quad (11)$$

$$\sum_{s\in\mathcal{S}} \vartheta_{ij,s} = \theta_{ij}^+ + \theta_{ij}^-,\ (i,j) \in \mathcal{E}, \quad (12)$$

$$0 \le \vartheta_{ij,s} \le \widehat{\theta}_{ij,s} - \widehat{\theta}_{ij,s-1},\ s \in \mathcal{S},\ (i,j) \in \mathcal{E}. \quad (13)$$

3) Nodal Power Balance Equations: The nodal active- and reactive-power balance equations are formulated as

$$P_i = -P_i^{\mathrm{d}} + \sum_{g\in\mathcal{G}_i} P_g^{\mathrm{e}} = \sum_{(i,j)\in\mathcal{E}} \Big(P_{ij} + \frac{P_{ij}^{\mathrm{loss}}}{2}\Big),\ i\in\mathcal{N}, \tag{14}$$

$$Q_i = -Q_i^{\mathrm{d}} + \sum_{g\in\mathcal{G}_i} Q_g^{\mathrm{e}} = \sum_{(i,j)\in\mathcal{E}} Q_{ij},\ i\in\mathcal{N}, \tag{15}$$

where P_i and Q_i respectively denote the net active- and reactive-power injections at node i, and losses in line (i,j) are represented by lumped loads distributed between the line sending and receiving ends.

B. Synchronous Generator Model

Using the classical machine model that comprises a constant voltage $E_g = 1+\Delta E_g$ with rotor electrical angular position δ_g behind reactance $\mathrm{j}X_g$, the active and reactive electrical power output of generator $g\in\mathcal{G}$ are calculated as

$$P_g^{\mathrm{e}} = \frac{E_g(\delta_g-\theta_i)}{X_g},\quad Q_g^{\mathrm{e}} = \frac{\Delta E_g - \Delta V_i}{X_g},\ g\in\mathcal{G}_i, \tag{16}$$

and they are limited through the following box constraints:

$$\underline{P}_g^{\mathrm{e}} \le P_g^{\mathrm{e}} \le \overline{P}_g^{\mathrm{e}},\quad \underline{Q}_g^{\mathrm{e}} \le Q_g^{\mathrm{e}} \le \overline{Q}_g^{\mathrm{e}},\ g\in\mathcal{G}_i. \tag{17}$$

Let ω_g and P_g^{m} respectively denote the electrical angular frequency and turbine mechanical power for generator $g\in\mathcal{G}$. Assuming that each generator initially operates at the synchronous steady state with $\omega_g(0) = \omega_{\mathrm{s}} = 2\pi 60\,[\mathrm{rad/sec}]$, we define $\Delta\omega_g := \omega_g - \omega_{\mathrm{s}}$. We model the dynamics of generator $g\in\mathcal{G}$ as follows:

$$\dot{\delta}_g = \Delta\omega_g,\ g\in\mathcal{G}, \tag{18}$$

$$M_g\Delta\dot{\omega}_g = P_g^{\mathrm{m}} - D_g\Delta\omega_g - P_g^{\mathrm{e}},\ g\in\mathcal{G}, \tag{19}$$

$$\tau_g\dot{P}_g^{\mathrm{m}} = P_g^{\mathrm{r}} - P_g^{\mathrm{m}} - R_g^{-1}\Delta\omega_g,\ g\in\mathcal{G}, \tag{20}$$

where M_g and D_g denote, respectively, its inertia and damping constants, and τ_g, P_g^{r}, and R_g denote its governor time constant, reference power input, and droop constant, respectively [18]. The generator model in (18)–(20) does not include dynamics for automatic voltage regulators or power-system stabilizers. Given the time scales of interest, however, we find that the model in (18)–(20) is *sufficiently accurate* to capture generator frequency dynamics. It is worth noting that dynamics of other components (like loads) can be easily incorporated at the expense of greater notational and computational burden.

III. Problem Formulation

Consider a scheduling horizon from time t_0 to t_0+T. We introduce two optimization time steps. The time step representing the faster system dynamics is denoted by $\Delta t^{\mathrm{D}} = \frac{T}{N^{\mathrm{D}}}$, which is small enough to capture the dynamics of generators and line power flows (e.g., $0.05\,[\mathrm{sec}]$). With Δt^{D}, the scheduling horizon subdivides into N^{D} intervals with the boundary points contained in the set $\mathcal{T}_{t_0}^{\mathrm{D}} = \{t_0, t_0+\Delta t^{\mathrm{D}},\ldots,t_0+T-\Delta t^{\mathrm{D}}\}$. Next, decisions on generator setpoints are made over longer time intervals $\Delta t^{\mathrm{S}} = \frac{T}{N^{\mathrm{S}}}$ (e.g., $2.5\,[\mathrm{sec}]$), and the scheduling horizon subdivides into N^{S} intervals with the boundary points contained in the set $\mathcal{T}_{t_0}^{\mathrm{S}} = \{t_0, t_0+\Delta t^{S},\ldots,t_0+T-\Delta t^{\mathrm{S}}\}$. In this section, we formulate the proposed dynamics-aware OPF problem and turn it into an LP problem to promote computational practicality.

A. Dynamics-aware OPF Problem with Linear Constraints

The dynamics-aware OPF problem minimizes the operation cost of generators over the scheduling horizon and penalizes deviations of generator angular frequency in the objective function. Define the positive-valued auxiliary variables $\Delta\omega_{g,t}^{+}$ and $\Delta\omega_{g,t}^{-}$ respectively representing upward and downward deviations of the generator g electrical angular frequency from the synchronous value. We formulate the following dynamics-aware OPF problem:

$$\min \sum_{t\in\mathcal{T}_{t_0}^{\mathrm{D}}}\sum_{g\in\mathcal{G}} \Big(C_g(P_{g,t}^{\mathrm{m}}) + \frac{\kappa}{|\mathcal{G}|}(\Delta\omega_{g,t}^{+}+\Delta\omega_{g,t}^{-})\Big)\Delta t^{\mathrm{D}} \tag{21a}$$

$$\text{s.t. } \frac{\delta_{g,t+\Delta t^{\mathrm{D}}}-\delta_{g,t}}{\Delta t^{\mathrm{D}}} = \Delta\omega_{g,t},\ t\in\mathcal{T}_{t_0}^{\mathrm{D}}, \tag{21b}$$

$$M_g\cdot\frac{\Delta\omega_{g,t+\Delta t^{\mathrm{D}}}-\Delta\omega_{g,t}}{\Delta t^{\mathrm{D}}} = P_{g,t}^{\mathrm{m}} - \Delta\omega_{g,t}D_g - P_{g,t}^{\mathrm{e}},\quad g\in\mathcal{G},\ t\in\mathcal{T}_{t_0}^{\mathrm{D}}, \tag{21c}$$

$$\tau_g\cdot\frac{P_{g,t+\Delta t^{\mathrm{D}}}^{\mathrm{m}}-P_{g,t}^{\mathrm{m}}}{\Delta t^{\mathrm{D}}} = P_{g,t'}^{\mathrm{r}} - P_{g,t}^{\mathrm{m}} - R_g^{-1}\Delta\omega_{g,t}\quad g\in\mathcal{G},\ t\in\mathcal{T}_{t_0}^{\mathrm{D}},\ t'\in\mathcal{T}_{t_0}^{\mathrm{S}}, \tag{21d}$$

$$\Delta\omega_{g,t} = \Delta\omega_{g,t}^{+} - \Delta\omega_{g,t}^{-},\quad \Delta\omega_{g,t}^{+},\Delta\omega_{g,t}^{-}\ge 0,\quad g\in\mathcal{G},\ t\in\mathcal{T}_{t_0}^{\mathrm{D}}, \tag{21e}$$

$$\delta_{1,t_0} = 0, \tag{21f}$$

$$\text{constraints (3)–(7), (10)–(17)}, \tag{21g}$$

where $C_g(P_{g,t}^{\mathrm{m}})$ represents the convex cost function of generator $g\in\mathcal{G}$ and $\kappa\ge 0$ is a uniform penalty factor for frequency deviations. Also, constraints in (21b)–(21d) are discrete-time dynamic equations derived from (18)–(20), and the constraint in (21f) sets the system reference angle. Furthermore, decision variables in the operational constraints (3)–(15), and (16)–(17) (all collected in (21g)) are augmented with subscript t, and the constraints are imposed for all time intervals $t\in\mathcal{T}_{t_0}^{\mathrm{D}}$.

B. Cost Function Linearization

The operation cost function $C_g(P_{g,t}^{\mathrm{m}})$, $g\in\mathcal{G}$, is typically a nonlinear convex function of its argument. In order to convert the dynamics-aware OPF problem in (21) into an LP problem, $C_g(P_{g,t}^{\mathrm{m}})$ is linearized as follows. Dividing the interval $[\underline{P}_g^{\mathrm{m}}, \overline{P}_g^{\mathrm{m}}]$ into H linearization segments indexed in the set $\mathcal{H} = \{1,\ldots,H\}$, each segment $h\in\mathcal{H}$ is delimited by its boundary values $\widehat{P}_{g,h-1}^{\mathrm{m}}$ and $\widehat{P}_{g,h}^{\mathrm{m}}$, such that $[\underline{P}_g^{\mathrm{m}}, \overline{P}_g^{\mathrm{m}}] = \bigcup_{h\in\mathcal{H}}[\widehat{P}_{g,h-1}^{\mathrm{m}}, \widehat{P}_{g,h}^{\mathrm{m}}]$, with end points $P_{g,0}^{\mathrm{m}} = \underline{P}_g^{\mathrm{m}}$ and $P_{g,H}^{\mathrm{m}} = \overline{P}_g^{\mathrm{m}}$. We associate the positive-valued auxiliary variable $p_{g,t,h}^{\mathrm{m}}$ to the linearization segment $h\in\mathcal{H}$ and calculate the cost function slope over the linearization segment as $\beta_{g,h} = \frac{C_g(\widehat{P}_{g,h}^{\mathrm{m}}) - C_g(\widehat{P}_{g,h-1}^{\mathrm{m}})}{\widehat{P}_{g,h}^{\mathrm{m}} - \widehat{P}_{g,h-1}^{\mathrm{m}}}$. The cost function is then linearizd as follows:

$$\widehat{C}_g(P_{g,t}^{\mathrm{m}}) = \sum_{h\in\mathcal{H}} \beta_{g,h}p_{g,t,h}^{\mathrm{m}},\ g\in\mathcal{G},\ t\in\mathcal{T}_{t_0}^{\mathrm{D}}, \tag{22}$$

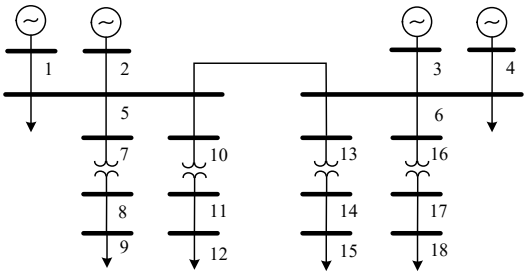

Fig. 1. One-line diagram for an 18-Bus shipboard test system [19].

TABLE I
DYNAMIC MODEL DATA OF GENERATORS/GOVERNORS

Generator g	M_g [sec]	D_g	τ_g [sec]	$\frac{1}{R_g}$
1	3.64	20	0.150	102.46
2	6.4	20	0.100	54
3	3.01	20	0.083	25
4	3.64	20	0.150	102.46

$$P^{\mathrm{m}}_{g,t} = \underline{P}^{\mathrm{m}}_{g} + \sum_{h\in\mathcal{H}} p^{\mathrm{m}}_{g,t,h},\ g\in\mathcal{G},\ t\in\mathcal{T}^{\mathrm{D}}_{t_0}, \tag{23}$$

$$0 \le p^{\mathrm{m}}_{g,t,h} \le \widehat{P}^{\mathrm{m}}_{g,h} - \widehat{P}^{\mathrm{m}}_{g,h-1},\ h\in\mathcal{H},\ g\in\mathcal{G},\ t\in\mathcal{T}^{\mathrm{D}}_{t_0}. \tag{24}$$

IV. CASE STUDIES

As a practical instance of islanded microgrids, we consider an 18-Bus AC shipboard test system, the one-line diagram for which is depicted in Fig. 1. Parameter values for lines, loads, and generator limits can be found in [19], and those for the generator dynamic model and quadratic cost function coefficients are reported in Tables I and II, respectively. Note that since we assume all four generators are online, the constant-term coefficient c_g does not affect the OPF solution. Thus, for simplicity, we set $c_g = 0$, for all $g \in \mathcal{G}$. The dynamic model time step is fixed as $\Delta t^{\mathrm{D}} = 0.05$ [sec] and the generator set-point decisions are made every $\Delta t^{\mathrm{S}} = 2.5$ [sec].

A. Benchmark Comparison Scenarios

We refer to the proposed dynamics-aware OPF problem in (21) modified with the linearized generator cost function described in (22)–(24) as "Case 0". We implement Case 0 in GAMS and use the CPLEX solver [20] to obtain the optimal generator set-points. We then apply the set-points as generator references in a dynamic simulation performed in PSAT [21], from which we obtain the associated time-domain trajectories of each generator's angular frequency and mechanical power. We compare these trajectories to the ones resulting by modulating optimal generator set-points from the solution of a standard dynamics-oblivious OPF problem for:

- Case 1: Generators are equipped with primary governor control, and system frequency is regulated with an industry-standard AGC (see, e.g., [8] for model details);
- Case 2: Generators are equipped with primary governor control, but there is no secondary frequency control.

For Cases 1 and 2, the mechanical power and angular frequency of generators are obtained from dynamic simulations of the 18-Bus test system in PSAT.

TABLE II
GENERATOR QUADRATIC COST FUNCTION COEFFICIENTS

Generator g	a_g [\$/(MWh)^2]	b_g [\$/MWh]	c_g [\$]
1	2.200	30	0
2	0.850	20	0
3	1.225	10	0
4	1.725	13	0

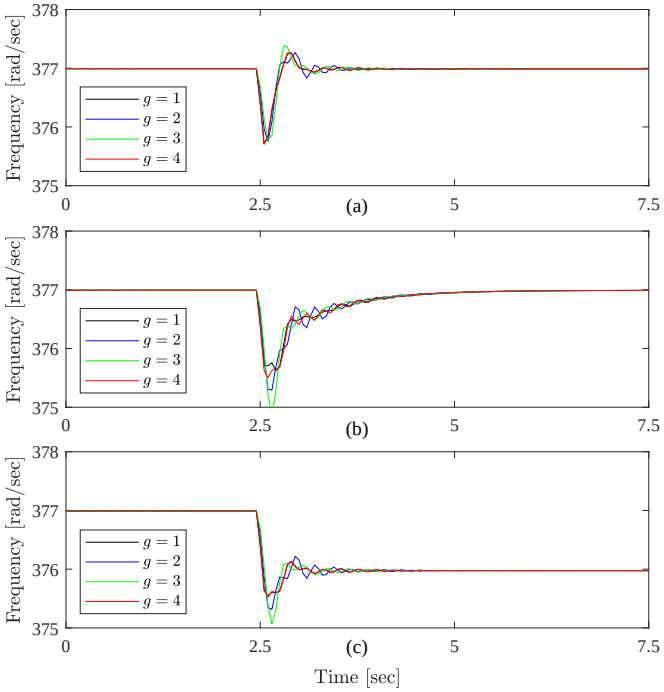

Fig. 2. Generator electrical angular frequency trajectories for (a) Case 0, (b) Case 1, (c) Case 2.

B. Load-change Disturbance

Let us consider a scheduling horizon of length $T = 7.5$ [sec] starting at time $t_0 = 0$ [sec]. At time $t = 2.5$ [sec] all the active-power loads in the system experience a 40% increase.

1) System Operation Cost & Generator Frequency: Given the quadratic cost function with coefficients reported in Table II and generator mechanical power trajectories, the operation costs for Cases 0, 1, and 2 are \$1.334, \$1.435, and \$1.249, respectively. Among the three cases considered, Case 2 bears the least operation cost as the AGC is not present to regulate frequency to synchronous value. Hence, as shown in Fig. 2c, we observe steady-state frequency deviations for all generators in Case 2. On the other hand, Case 1 embeds a standard AGC system, which maintains generator frequency to be the synchronous value at steady state, as shown in Fig. 2b. However, Case 1 incurs the highest operation cost of all three cases. This is because the standard AGC adjusts generator references via an ad-hoc approach contingent on small-signal assumptions, which may be invalidated by the large load disturbance considered in our simulations. Finally, Case 0 recovers generator frequency trajectories back to the synchronous value at steady state with 7.04% savings in operation cost as compared to Case 1. Furthermore, a visual inspection of Figs. 2a–2b reveals that, in Case 0, the generator frequency trajectories settle back to steady state faster and

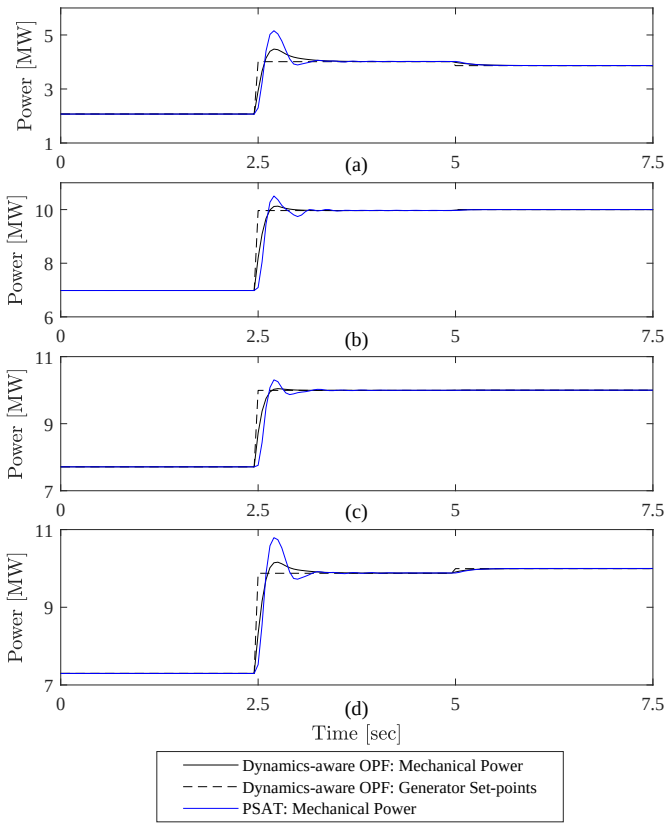

Fig. 3. Mechanical power and reference set-points in Case 0 for (a) generator 1, (b) generator 2, (c) generator 3, and (d) generator 4.

with less initial frequency nadir, indicating better dynamic performance overall.

2) Mechanical Power & Set-points: Here, we offer further details for the results in Case 0. In Fig. 3, we plot trajectories of the optimal generator set-points and the generator mechanical power obtained from the dynamics-aware OPF problem as the dashed-black and the solid-black traces, respectively. Indeed, we find that the slower decisions on generator set-points are made for each longer time interval of $\Delta t^{\mathrm{S}} = 2.5\,[\mathrm{sec}]$, while generator dynamics are captured at the faster time-scale corresponding to the shorter time interval of $\Delta t^{\mathrm{D}} = 0.05\,[\mathrm{sec}]$. In the same figure, we also overlay the *actual* trajectories of generator mechanical power obtained from a PSAT simulation using the optimal set-points (i.e., the dashed traces) as the generator references. We observe that the trajectories from the dynamics-aware OPF match closely to the PSAT simulation in steady state, providing validation for the proposed formulation. During the transient period prior to reaching steady state, the two sets of mechanical power trajectories follow similar trends. Mild differences are likely due to the simplified reduced-order generator dynamical models and linearized power flow constraints adopted to reduce computational burden of the dynamics-aware OPF problem.

V. Concluding Remarks

In this paper we formulated a linear dynamics-aware OPF problem for islanded microgrid operation aimed at bridging the gap amongst hierarchical control layers through co-optimization of energy dispatch and frequency regulation. The proposed multi-time-scale model embeds discrete-time generator dynamics and a linearized power flow model as constraints. The numerical results demonstrate the effectiveness of the proposed model in reducing the microgrid operation cost during the transient period after a load disturbance and improving system frequency response. Future work includes consideration for energy storage and load forecast uncertainty.

References

[1] D. T. Ton and M. A. Smith, "The U.S. department of energy's microgrid initiative," *Electricity J.*, vol. 25, no. 8, pp. 84–94, Oct. 2012.

[2] P. Voss and C. Kurnik, "Financing microgrids in the federal sector," Nat. Renewable Energy Lab.(NREL), Golden, CO, USA, Tech. Rep., 2020. [Online]. Available: http://https://www.nrel.gov/docs/fy20osti/77559.pdf

[3] A. Aram, "Microgrid market in the USA," *Hitachi Rev.*, vol. 2630, 2017.

[4] P. Kaluza, A. Kölzsch, M. T. Gastner, and B. Blasius, "The complex network of global cargo ship movements," *J. Roy. Soc. Interface*, vol. 7, no. 48, pp. 1093–1103, 2010.

[5] M. Farrokhabadi, C. A. Cañizares, and K. Bhattacharya, "Frequency control in isolated/islanded microgrids through voltage regulation," *IEEE Trans. Smart Grid*, vol. 8, no. 3, pp. 1185–1194, May 2015.

[6] G. Shahgholian, "A brief review on microgrids: Operation, applications, modeling, and control," *Int. Trans. Elect. Energy Syst.*, p. e12885, 2021.

[7] A. Bidram and A. Davoudi, "Hierarchical structure of microgrids control system," *IEEE Trans. Smart Grid*, vol. 3, no. 4, pp. 1963–1976, Dec. 2012.

[8] S. V. Dhople, Y. C. Chen, A. Al-Digs, and A. D. Domínguez-García, "Reexamining the distributed slack bus," *IEEE Trans. Power Syst.*, vol. 35, no. 6, pp. 4870–4879, Nov. 2020.

[9] N. Li, C. Zhao, and L. Chen, "Connecting automatic generation control and economic dispatch from an optimization view," *IEEE Trans. Control Netw. Syst.*, vol. 3, no. 3, pp. 254–264, Sep. 2016.

[10] D. Cai, E. Mallada, and A. Wierman, "Distributed optimization decomposition for joint economic dispatch and frequency regulation," *IEEE Trans. Power Syst.*, vol. 32, no. 6, pp. 4370–4385, Nov. 2017.

[11] T. Stegink, C. De Persis, and A. van der Schaft, "A unifying energy-based approach to stability of power grids with market dynamics," *IEEE Trans. Autom. Control*, vol. 62, no. 6, pp. 2612–2622, Jun. 2017.

[12] T. Stegink, A. Cherukuri, C. De Persis, A. Van der Schaft, and J. Cortés, "Hybrid interconnection of iterative bidding and power network dynamics for frequency regulation and optimal dispatch," *IEEE Trans. Control Netw. Syst.*, vol. 6, no. 2, pp. 572–585, Jun 2019.

[13] G. Zhang, J. McCalley, and Q. Wang, "An AGC dynamics-constrained economic dispatch model," *IEEE Trans. Power Syst.*, vol. 34, no. 5, pp. 3931–3940, Sep. 2019.

[14] R. Khatami, M. Parvania, C. Chen, S. S. Guggilam, and S. V. Dhople, "Dynamics-aware continuous-time economic dispatch: A solution for optimal frequency regulation," in *Proc. 53rd Hawaii Int. Conf. Syst. Sci.*, 2020, pp. 3186–3195.

[15] M. Bazrafshan, N. Gatsis, A. F. Taha, and J. A. Taylor, "Coupling load-following control with OPF," *IEEE Trans. Smart Grid*, vol. 10, no. 3, pp. 2495–2506, May 2019.

[16] H. Zhang, V. Vittal, G. T. Heydt, and J. Quintero, "A relaxed AC optimal power flow model based on a Taylor series," in *Proc. IEEE Innov. Smart Grid Technol.-Asia*, 2013, pp. 1–5.

[17] M. Carrión and J. M. Arroyo, "A computationally efficient mixed-integer linear formulation for the thermal unit commitment problem," *IEEE Trans. Power Syst.*, vol. 21, no. 3, pp. 1371–1378, Aug. 2006.

[18] P. W. Sauer and M. A. Pai, *Power System Dynamics and Stability*. Upper Saddle River, NJ, USA: Prentice-Hall, 1998.

[19] T. L. Baldwin and S. A. Lewis, "Distribution load flow methods for shipboard power systems," *IEEE Trans. Ind. Appl.*, vol. 40, no. 5, pp. 1183–1190, Sep./Oct. 2004.

[20] The ILOG CPLEX, 2018. [Online]. Available: http://www.ilog.com/products/cplex/

[21] F. Milano, "An open source power system analysis toolbox," *IEEE Trans. Power Syst.*, vol. 20, no. 3, pp. 1199–1206, Aug. 2005.